Long Time Dynamic Simulations: Exploring the Folding Pathways of an Alzheimer's Amyloid Aβ-Peptide

JOHN E. STRAUB,*,† JAVIER GUEVARA,†,‡ SHUANGHONG HUO,†,§ AND JONATHAN P. LEE†

Department of Chemistry, Boston University, Boston, Massachusetts 02215, Escuela de Ciencia y Tecnologia, Universidad de San Martin, Alem 3901 (1651) San Andres, Argentina, and Gustaf H. Carlson School of Chemistry and Biochemistry, Clark University, Worcester, Massachusetts 01610

Received October 4, 2001

ABSTRACT

We describe the MaxFlux algorithm for the computation of likely pathways for global macromolecular conformational transitions. The algorithm assumes an overdamped diffusive dynamics for the biomolecule, appropriate to large scale conformational changes. As an application of the MaxFlux method, we explore conformational transitions between α-helical, collapsed coil, and β-sheet conformations of an amyloid Aβ-peptide. The resulting transition pathways are analyzed in terms of the mechanism of conformational transition and the progression of the peptide energetics in both an aqueous and a membrane-mimicking nonpolar solvent.

1. Introduction

We provide an account of recent efforts to develop and apply computational methods for the study of large scale conformational changes in peptides and proteins. A summary of the MaxFlux method for the computation of likely transition pathways is presented. Application of the MaxFlux method to the problem of characterizing conformational changes intrinsic to the aggregative activity of the Alzheimer's amyloid β-peptide is discussed in detail.

1.1 Computation of Long Time Diffusional Biomolecular Dynamics. Computational studies using molecular dynamics of atomistic models have reached the microsecond time scale.[1−3] However, routine simulations of moderately sized, solvated peptides are currently limited to the nanosecond time scale. The sort of conformational transition that must take place in the amyloid peptide occurs on a time scale of microseconds or longer.[4,5]

An alternative to the use of molecular dynamics is to compute a variationally optimized dynamical trajectory connecting fixed end points of known structure. For example, we can connect the (initial) alcoholic α-helical peptide structure with the (final) aqueous coil peptide structure using a chain of imagined structural intermediates. If we assume that the molecule's motion is diffusive, we can hold the initial and final structures fixed while varying the intermediates and ask, "Which chain of intermediates, or which reaction pathway, corresponds to the fastest transition between the chosen initial and final states?" Stated differently, "What is the pathway of maximum reactive flux connecting the initial and final peptide conformations?" Those questions are addressed in this work through the application of the MaxFlux algorithm.[5−7]

1.2 Structure and Activity of the Aβ-Peptide. The amyloid β-peptide is found to be the principal component of plaques and fibrils found in the brains of many patients that suffer the symptoms of Alzheimer's disease. The "Aβ hypothesis" proposes that the β-peptide plays a central role as the pathogenic agent in Alzheimer's disease.[8,9] There have been significant recent advances in the experimental[4,10−15] and theoretical[16,17] study of the amyloid β-peptide and the thermodynamics and kinetics of amyloid plaque formation. The tendency of these peptides to aggregate is the cause of their significance to human health. Their typical insolubility is a serious impediment to their experimental study. Early studies of the Aβ-peptide's solution structure using NMR were limited to unnatural, alcoholic solvents.[18−20] Solvents such as trifluoroethanol/water mixtures increase peptide solubility but also favor helical structure. It was not surprising that the 1−40 β-amyloid peptide was found to have significant helical content in alcoholic solvent.[20] Studies of the amyloid fibrils using fiber diffraction indicated that the peptide was, in its predominate form, aggregated in a β-sheet motif.[21,22] The combination of these studies led to a model for plaque formation in which a largely α-helical peptide undergoes a conformational transition to a less soluble β-sheet structure, which then deposits as plaque.[23,24]

How accurately does this model describe in vivo plaque formation? Recent advances have made it possible to

John E. Straub was born in Denver, CO, on April 11, 1960. He received his B. S. degree in 1982 from the University of Maryland at College Park, where he worked with Millard Alexander, and his Ph.D. degree in 1987 from Columbia University, working under the direction of Bruce Berne. Following an NIH postdoctoral fellowship with Martin Karplus at Harvard University, in 1990 he joined the faculty of the Chemistry Department of Boston University.

Javier Guevara was born in Buenos Aires, Argentina, on April 14, 1963. He received his undergraduate and doctoral degrees in physics from the University of Buenos Aires. He is currently an Assistant Professor of Physics at the University of San Martin in Argentina.

Shuanghong Huo was born in Beijing, People's Republic of China, on October 24, 1967. She received her undergraduate degree in Chemistry from Peking University, her doctoral degree from Boston University, working with John E. Straub, and was a postdoctoral fellow in the laboratory of Peter Kollman at the University of California, San Francisco. She is currently Assistant Professor of Chemistry at Clark University.

Jonathan P. Lee was born in Watertown, NY, on February 17, 1959. He received his B. S. degree in 1981 from St. Lawrence University and his doctoral degree from The Ohio State University in 1987. The following year, he was a visiting faculty member at Wuhan University in the People's Republic of China. He served as a lecturer in the Department of Biological Chemistry and Molecular Pharmacology at Harvard Medical School from 1988 until 1994 when he joined the faculty of the Chemistry Department at Boston University.

† Boston University.
‡ Universidad de San Martin.
§ Clark University.

10.1021/ar010031e CCC: $22.00
Published on Web 05/09/2002

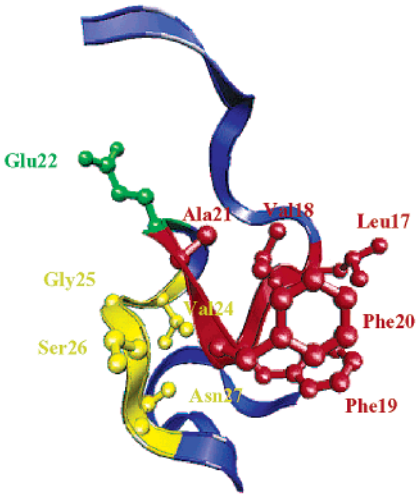

FIGURE 1. The wild type form of the congener amyloid β(10−35)-NH_2 peptide determined experimentally[10,15] for the peptide in aqueous solution. From the N-terminus, the groups are Tyr10-Glu11-Val12-His13-His14-Gln15-Lys16 (blue), Leu17-Val18-Phe19-Phe20-Ala21 (red), Glu22 (green), Asp23 (blue), Val24-Gly25-Ser26-Asn27 (yellow), Lys28-Gly29-Ala30-Ile31-Ile32-Gly33-Leu34-Met35 (blue).

explore the structures of Aβ(1−40) and Aβ(10−35) in aqueous solution (see Figure 1).[10,15] These studies provide us with more reliable estimates of the dominant structural characteristics of the in vivo peptide. As we would expect, the structure in aqueous solution lacks the helical character of the 1−40 peptide in alcoholic solvent.[20] However, there are also significant similarities between the two peptide structures.

These experimental results lead to questions of fundamental biophysical significance. The peptide structure and solubility is strongly dependent on solvent.[10,20,25,26] How can we characterize the solution phase structures of the peptide and which factors determine its solubility? What are the pathways of conformational change that connect the peptide structures in aqueous and nonpolar membrane environments? In the process of peptide deposition, how can we characterize conformational transition pathways from the solution structure to the β-sheet structure assumed in the plaque?

In this Account, we present the MaxFlux algorithm and discuss the underlying assumptions on which the method rests. Important details related to the practical application of the method are discussed in the context of the computation of dominant reaction pathways for conformational transitions in the Aβ-peptide. Our simulation model combines an atomistic representation of the peptide[27] with a surface-area-based mean force solvation potential developed[28] to approximate solvation effects without explicit solvent. The results allow us to recognize regions of conserved structure and suggest a mechanism for the conformational transitions between helical, coiled, and sheet conformations that may be central to the nature of the peptide's solubility and propensity for formation of amyloid fibrils.

2. Long Time Diffusional Dynamics from the MaxFlux Method

The development of general computational methods for the investigation of long time scale dynamical processes is an active area of research. A review of that field is beyond the scope of this account, but has been reported elsewhere.[5,29,30] Huo and Straub have proposed a method for identifying probable pathways for conformational transitions in biomolecular systems. The MaxFlux algorithm is designed to variationally optimize a reaction pathway connecting known initial (reactant) and final (product) peptide structures in such a way that the transition time for moving between the reactant and product conformations is minimized. The pathway is described by a series of $M - 1$ intermediate peptide structures and the end points. These $M + 1$ structures are located at a series of positions $\mathbf{R} = (\mathbf{r}_R,\mathbf{r}_1...\mathbf{r}_{M-1},\mathbf{r}_P)$ along a pathway connecting reactant ($\mathbf{r}_R$) and product ($\mathbf{r}_P$). Here, each $\mathbf{r}$ represents a complete list of coordinates of all of the peptide atoms defining a given peptide conformation. In this way, the pathway is divided into M shorter segments defined by intermediate structures along the transition pathway. A function is defined that is a measure of the reaction time required to undergo a transition between the reactant and product conformations by an overdamped diffusional Brownian dynamics

$$\sum_{k=0}^{M-1} f(\mathbf{r}_k)|\mathbf{r}_{k+1} - \mathbf{r}_k| \qquad (1)$$

$|\mathbf{r}_{k+1} - \mathbf{r}_k|$ is a measure of how far the peptide has moved between the previous and current positions. $f(\mathbf{r}_k)$ is a measure of the time required for the peptide to move some unit distance near its conformation r_k. It follows that $f(\mathbf{r}_k)|\mathbf{r}_{k+1} - \mathbf{r}_k|$ is a function that is small in regions where the peptide's diffusive motion is most rapid and large in regions where the peptide's diffusive motion is slow. This means that $f(\mathbf{r}_k)|\mathbf{r}_{k+1} - \mathbf{r}_k|$ is an inverse flux or a measure of the time required to move from position $\mathbf{r}_k$ to $\mathbf{r}_{k+1}$. The sum over all M segments of the path is a measure of the reaction time for moving from the reactant to the product conformation.

The form for $f(\mathbf{r})$ is built on three assumptions. The first is that the motion of the peptide is diffusive and that inertial motion associated with high frequency bond and angle stretching motion can be ignored. The peptide will have three forces acting on it: the conservative force due to the interaction potential, the frictional force proportional to the velocity, and the random force. The conservative force is due to the interaction of atoms of the peptide that are explicitly included in our model. The friction and random force mimic the effect of the solvent that is treated implicitly in the computational model. The frictional force can remove energy from the system only through a frictional damping of the velocity. The frictional dissipation is related to the random force in such a way that the correct temperature (kinetic energy) is maintained on average in the peptide.

With our simulations, we hope to explore the dynamics of large scale conformational transitions in the solvated peptide. The nature of the motions in a dense solvent environment is expected to be diffusive, because they occur on a long time scale in which inertial motion will be damped out by repeated collisions with the solvent molecules. This assumption of diffusive motion should be reasonable for long peptides undergoing transitions that take many nanoseconds or microseconds to complete.

The second assumption is that the magnitude of the flux along the trajectory connecting the reactant and product conformation is constant; that is, that at steady-state we can expect a rate of conversion between the reactant and product states that is constant along the given transition pathway. Berkowitz et al.[31] proposed that the resistance to diffusive motion is proportional to

$$f(\mathbf{r}) = \mathrm{e}^{W(\mathbf{r})/k_\mathrm{B}T} \tag{2}$$

where the effective potential $W(\mathbf{r}) = U(\mathbf{r}) + k_\mathrm{B}T \ln(\gamma(\mathbf{r})/\gamma(\mathbf{r}_\mathrm{R}))$. This effective potential combines the bare peptide and solvent potential $U(\mathbf{r})$ with a logarithmic function of the friction $\gamma(\mathbf{r})$ at point $\mathbf{r}$ relative to the friction at some arbitrarily chosen reference point $\gamma(\mathbf{r}_\mathrm{R})$. If we further assume that the friction is constant, the effective potential $W(\mathbf{r}) = U(\mathbf{r})$ and the time to move some local distance $\mathrm{dl}(\mathbf{r})$ will be proportional to $\exp[U(\mathbf{r})/k_\mathrm{B}T]$.

We expect the reaction time to be proportional to $\sqrt{m/k_\mathrm{B}T}$ (or the inverse of the average velocity along the one-dimensional path). The time should also be inversely proportional to the frequency of motion in the basin of reactant conformers ω_0 as a measure of the entropy of the reactant state conformations. The reaction time should also be proportional to the friction γ. Therefore, our function $f(\mathbf{r})$ takes the final form

$$f(\mathbf{r}) = \frac{\gamma}{\omega_0}\left(\frac{2\pi m}{k_\mathrm{B}T}\right)^{1/2} \mathrm{e}^{U(\mathbf{r})/k_\mathrm{B}T} \tag{3}$$

The prefactor has the units of time divided by length. Although the prefactor may differ for "open" and "closed" states of a peptide, the greatest variation in $f(\mathbf{r})$ will result from changes in $U(\mathbf{r})$. In practice, we will ignore changes in the prefactor and consider it to be constant.

When multiplied by the increment of length in eq 1, the result is an approximate reaction time. We imagine that the most important pathways leading from reactant to product will correspond to small values of this function—small values of the reaction time. The MaxFlux algorithm is designed to minimize the reaction time and isolate the dominant reaction pathways for a given conformational transition between known reactant and product conformations.

The objective is to minimize eq 1 by adjusting the positions of the intermediate structures forming the pathway, all the while restraining the distances between successive intermediate structures in the chain (the $|\mathbf{r}_{k+1} - \mathbf{r}_k|$ or $\mathrm{dl}(\mathbf{r})$ increments) to be the same. Following the computational protocol of Elber and co-workers,[32] we add restraints (1) to restrain the mean-square distances between successive intermediate structures to be approximately constant,

$$C_\mathrm{A}(\mathbf{R}) = \kappa \sum_{k=1}^{M} [(\mathbf{r}_k - \mathbf{r}_{k-1})^2 - d_\mathrm{av}^2]^2 \tag{4}$$

where $d_\mathrm{av}^2 = \sum_{k=1}^{M}(\mathbf{r}_k - \mathbf{r}_{k-1})^2/M$, (2) to discourage intermediates from coming close to one another

$$C_\mathrm{R}(\mathbf{R}) = \frac{\rho}{\lambda} \sum_{j>k+1} \exp[-\lambda(\mathbf{r}_j - \mathbf{r}_k)^2/<d>^2] \tag{5}$$

and (3) to eliminate rigid body translations and rotations[32]

$$\sum_{\mu=1}^{N} m_\mu(\mathbf{r}_\mu - \mathbf{r}_\mu^\mathrm{fix}) = 0 \tag{6}$$

$$\sum_{\mu=1}^{N} m_\mu \mathbf{r}_\mu \times \mathbf{r}_\mu^\mathrm{fix} = 0 \tag{7}$$

where N is the number of atoms in the system, m_μ is the atomic mass, and $\mathbf{r}_\mu$ is the Cartesian coordinates for the μth atom. $\{\mathbf{r}_\mu^\mathrm{fix}\}_{\mu=1,N}$ is the arithmetic average of the coordinates of the atoms in the reactant and product conformations.

2.1 Fixed End Points for the Transition Pathways. We have computed reaction pathways connecting four peptide structures of (1) the experimentally derived collapsed coil conformer of Aβ(10−35)-NH_2 in water,[15] (2) the experimentally derived helical structure of Aβ(1−40) in TFE/water mixture[20] truncated to Aβ(10−35)-NH_2, (3) the modeled extended, and (4) the hypothetical folded structure proposed for intermolecular β-sheet formation.[33] The extended structure was generated with Insight II.[34]

In the model helical structure, there are two helices extending over the regions Q15 K16 L17 V18 F19 F20 A21 E22 D23 and I31 I32 G33 L34 M35. Other regions may be referred to as coil. In the collapsed coil structure, there is a hydrophobic cluster extending over the sequence L17 V18 F19 F20 A21. In the collapsed coil structure of the Aβ(1−40) peptide, residues 1−9 and 36−40 are relatively disordered.[15] In each of the compact structures, there is a turn in the region V24 G25 S26 N27.

We examined conformational transition pathways connecting each pair of the Aβ(10−35)-NH_2 peptide structures

$$\begin{aligned}\text{collapsed coil}_{(\text{water})} &\leftrightarrow \text{helical structure}_{(\text{TFE/water})} \leftrightarrow \\ &\text{extended}_{(\text{model})} \leftrightarrow \text{collapsed coil}_{(\text{water})} \leftrightarrow \\ &\beta\text{-sheet}_{(\text{model})} \leftrightarrow \text{extended}_{(\text{model})}\end{aligned}$$

Both the collapsed coil and helical structures have the common feature of a flexible N-terminal region extending over residues Y10 E11 V12 H13 H14. We have isolated energy minima associated with each conformational geometry, indicating that for our model, both conformational states represent basins of thermodynamically (meta) stable peptide states.

2.2 Initial Guess for the Transition Pathways. The collapsed coil, the helical structure, and the putative

extended and folded β-sheet structures were treated with steepest descent energy minimization to relieve bad steric contacts while maintaining the minimized peptide structures close to the experimentally derived NMR structures.[15,20] A linear interpolation in $\psi-\phi$ space was performed to construct the initial guess of the conformational transition pathways connecting the "reactant" and "product" states. Ten intermediate structures were generated along each path. Steepest descent energy minimization with constrained ϕ and ψ dihedral angles was performed after each of the linear interpolations, followed by a moderate amount of adapted basis Newton−Raphson constrained energy minimization[27] where the peptide bond dihedral angle was restrained to be roughly 180°.

2.3 Quasiannealing of the Transition Pathway. After the linear interpolation, the effective energy was always relatively high, and the violation of the equal distance and self-avoidance restraints was great. We optimized each transition pathway to find the minimum estimated transition time using a "quasiannealing" procedure. The reciprocal temperature $1/k_BT$ was increased from 0.01 to 0.05, and finally, to 0.1 mol/kcal. At each temperature, conjugate gradient energy minimization was performed. The parameter λ was set to 2.0; parameters κ and ρ in eqs 4 and 5 were set by trial and error. The range of values used was $\kappa\in$[100,4000] and $\rho\in$[2000,4000].

Following the initial effort to optimize the pathway between fixed end points for each transition using the quasiannealing procedure, additional trajectories were generated in the neighborhood of each optimal pathway, and the estimate of the diffusional transition time was minimized according to the MaxFlux protocol. This resulted in a bundle of 20 transition pathways connecting the fixed initial and final conformations along each segment. The general character of each transition is shared by each transition pathway. Differences in the pathway energetics indicate the local ruggedness of the potential energy landscape. Note that we cannot assume that the transition pathways are "optimal". The development of more effective methods for the refinement of the transition pathways is an important outstanding problem.

The final optimized paths correspond to the high temperature ($1/\beta$) reaction paths. Minimization of the target function plus restraints resulted in a final pathway that had a small value of the reaction time. For the final optimized pathway, the restraints were insignificant in comparison to the contribution of eq 1.[6,7]

3. Simulation Model of the Solvated Aβ Peptide in Aqueous and Nonaqueous (Octane) Solvent

An atomistic model of Aβ(10−35) was simulated for the sequence YEVHH QKLVF FAEDV GSNKG AIIGL M. The protonation states of the titratable residues were taken to be the dominant states of the aqueous solvated peptide at pH 7. The CHARMM force field was used with version 19 parameter set.[27] In building the peptide, the $-NH_2$ of the N-terminus and the $-CONH_2$ of the C-terminus were added along with the corresponding bond and bond angle parameters. A distance-dependent dielectric constant was employed to model the solvent screening, and the nonbonded interactions were truncated using the standard cutoff for the version 19 force field.[35]

Table 1. Atomic Solvation Parameters ($\Delta\sigma$) for Water and Octane, in cal mol^{-1} A^{-2} [a]

atom type	water	octane
aliphatic C	20	−6
aromatic C	−1	−30
hetero C	−22	−34
S	32	−9
O	−83	−68
O^-	−128	−114
N	−140	−132
N^+	−198	−178

[a] From ref 38.

A solvation energy function[28] was combined with the CHARMM potential energy. The solvation model assumes that the solvation free energy of a given atom in the peptide is proportional to the atom's solvent accessible surface area (ASA) through the atomic solvation parameter ($\Delta\sigma$) as[36]

$$E_{\text{solv}} = \sum_{i=1}^{N} \Delta\sigma_i \text{ASA}_i \tag{8}$$

with ASA_i and $\Delta\sigma_i$ being the ASA and $\Delta\sigma$ of the atom i respectively, and N being the total number of atoms in the peptide. $\Delta\sigma$ comes either from the experimental water−octanol free energies of transfer for amino acids or from statistical analysis of known protein structures applied to globular proteins.[37] We chose the atomic solvation parameters shown in Table 1, where there are three different types of carbon atoms: aliphatic, aromatic, or hetero (a C attached to any number of heteroatoms).[38] The probe radii for water and octanol were both taken to be equal to 1.4 A. There are two important features of the solvation parameters. First, the atomic solvation parameter for the aliphatic C and S atoms are positive (hydrophobic), whereas all others are negative (hydrophilic). Second, the magnitude of the atomic solvation parameters of C and S are roughly five times smaller than those of the polar atoms N and O and the ions O^- and N^+.

Alternative implicit solvation models do exist. However, those models lacked complementary parameters for aqueous and nonaqueous solvation. The qualitative features presented in this work are not found to depend sensitively on the choice of solvation model. Any implicit solvent model may be readily employed with the MaxFlux method.

4. Characteristics of Computed Trajectory "Bundles"

We examined conformational transition pathways connecting the α-helical peptide conformation observed in an alcoholic solvent, the collapsed coil conformation observed in an aqueous solution, and the model extended state and folded β-sheet conformations consistent with β-sheet formation observed in fibrillar aggregates.

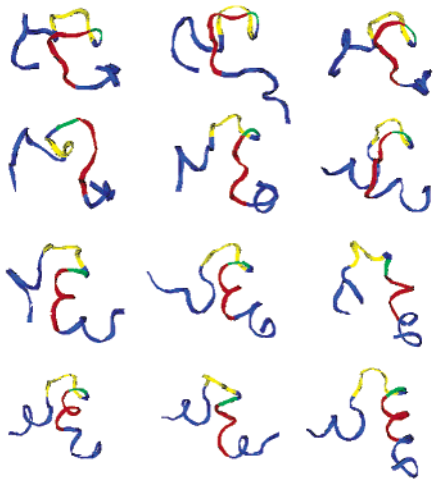

FIGURE 2. Structures along an optimized transition pathway connecting the collapsed coil NMR structure (upper left) and the α-helical structure (lower right) modeled on the NMR structure for the 1−40 Aβ peptide found in TFE/water solution modeled in aqueous solution. The figure should be read as in English text, from upper left to lower right.

4.1 Collapsed Coil → α-Helix Transition Pathways. A transition pathway of the conformational transition from collapsed coil to helix is shown in Figure 2. Each represented structure is an intermediate structure along the transition pathway. (In this context, the term "intermediate" does not necessarily imply that the structure represents a metastable kinetic intermediate.) The helical segment was defined as three continuous residues having a helical conformation. The first helical segment forms midway through the transition in E22 D23 V24, a region adjacent to the central hydrophobic cluster (L17 V18 F19 F20 A21). However, this helical segment is not stable. It is disrupted and then forms again in the ninth intermediate conformer. Subsequently, the second helical segment forms at L17 V18 F19 inside the central hydrophobic cluster.

In the refined transition path, two important features emerge. The first feature is that in all computed trajectories, there is no significant conformational change near G25 until the transition is beyond the midpoint of the pathway. Prior to that point, the reaction pathway fluctuates about the collapsed coil conformation. Subsequently, a series of dihedral transitions mark the initiation of large scale structural changes.

The second common feature is a cascade of large transitions in the backbone torsional angles from G25 to the N terminus. The cascade is initiated near L17 and V24 and propagates outward toward the N terminus. The latter half of the transition is best characterized by the large, concerted fluctuations around K28, G29, A30, and I31. K28 and G29 are within a coil region of the helical structure,[20] whereas A30 and I31 are at the beginning of the second helical segment. The unstable feature of the structure about the I31 helical segment also appeared in the analysis of helix formation.[20]

The trajectory bundle demonstrates a significant degree of structural similarity between the collapsed coil and the helical structure in the region of G25 S26 N27. This structural similarity was conserved over the entire transition pathway. This observation coincides with a previous NMR study of Aβ(1−28) E22Q in DMSO that identified a turn starting at residue 25.[39] Coles and co-workers[26] observed a kink near G25−N27 in the water−micelle environment; however, Sticht et al.[20] did not report G25−S26 as a turn in their Aβ(1−40) TEF/water system.

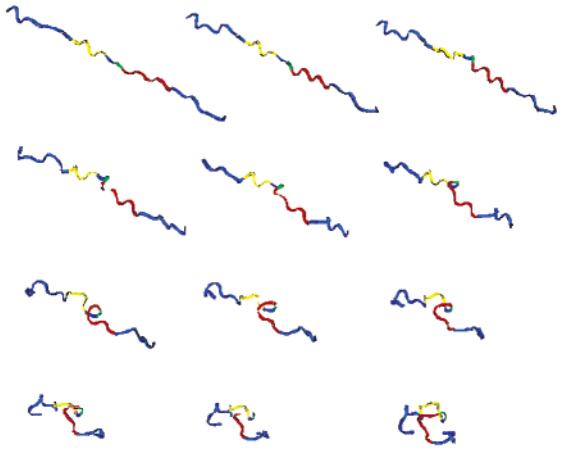

FIGURE 3. Structures along an optimized transition pathway connecting the collapsed coil NMR structure (lower right) and the model extended conformation (upper left) modeled in aqueous solution.

4.2 Collapsed Coil → Extended State Transition Pathways. Throughout this transition, depicted for one of twenty computed pathways in Figure 3, the amino terminus up to Q15 is very flexible, and the extension of the central hydrophobic cluster E22 D23 V24 undergoes a large torsional angle transition at the beginning of the conformational change. Subsequently, the region of ongoing transition expands to include the central hydrophobic cluster L17 V18 F19 F20 A21. The I31 dihedral angles show a large transition near the sixth intermediate marking a break in the short helical turn at the C-terminus. In contrast, the turn region around G25 S26 undergoes relatively small variations in the backbone dihedral angles. We observe that G25 loses the nonbonded contacts present in the collapsed coil relatively late along the pathway.

4.3 α-Helix → Extended State Transition Pathways. The computed transition pathways, one of which is depicted in Figure 4, do not include the collapsed coil as an intermediate on the conformational transition pathway from the helical structure to the extended state. The final path is shown in Figure 4. Unlike the transition from the collapsed coil to the extended state, the region V24 G25 S26 undergoes a large change from the second to the third intermediate structure. This turn forms the lead (or terminal) end of the helical segment and forms early in the transition from the extended to the helical conformation. Unwinding of the helix is correlated with a series of dihedral angle fluctuations beginning at residue V18 and propagating forward through V24. The large conformational change in the turn region is related to the decomposition of the helix at V24.

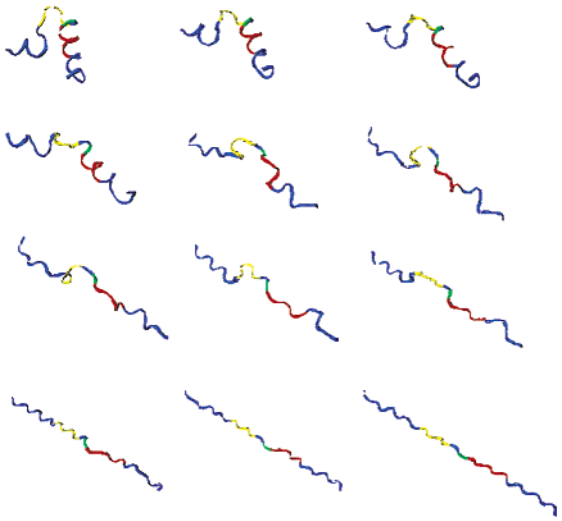

FIGURE 4. Structures along an optimized transition pathway connecting an α-helical target (upper left) modeled on the NMR structure for the 1−40 Aβ peptide (lower right) found in TFE/water solution and the model extended conformation.

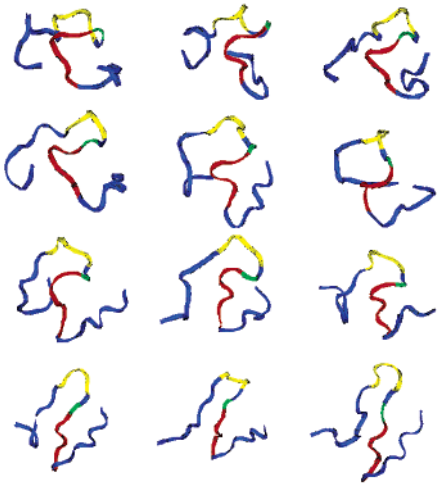

FIGURE 5. Structures along an optimized transition pathway connecting the collapsed coil state (upper left) and a modeled folded β-sheet target conformation (lower right) in aqueous polar solvent.

4.4 Collapsed Coil → β-Sheet Transition Pathways. We have computed pathways for the transition from the collapsed coil conformation, experimentally observed to be the dominant structural form in aqueous solution, to the putative β-sheet structure, consistent with a proposed model fibrillar structure.[33] A representative transition pathway is shown in Figure 5. A common feature of the computed trajectories is the conservation of the VGSN turn region throughout the transition from collapsed coil to putative β-sheet structure.

Corroborating evidence for the importance of this conformationally invariant region comes from chemical shift data derived from 2D-NMR spectra measured for the peptide in aqueous solution at 15, 25, and 35 °C.[40] The VGSNKG region of Val24 through Gly29 shows little variation in chemical shift between 5 and 35 °C. This suggests that the structure of that region in aqueous solution is quite stable and is disrupted little by the significant elevation in temperature.

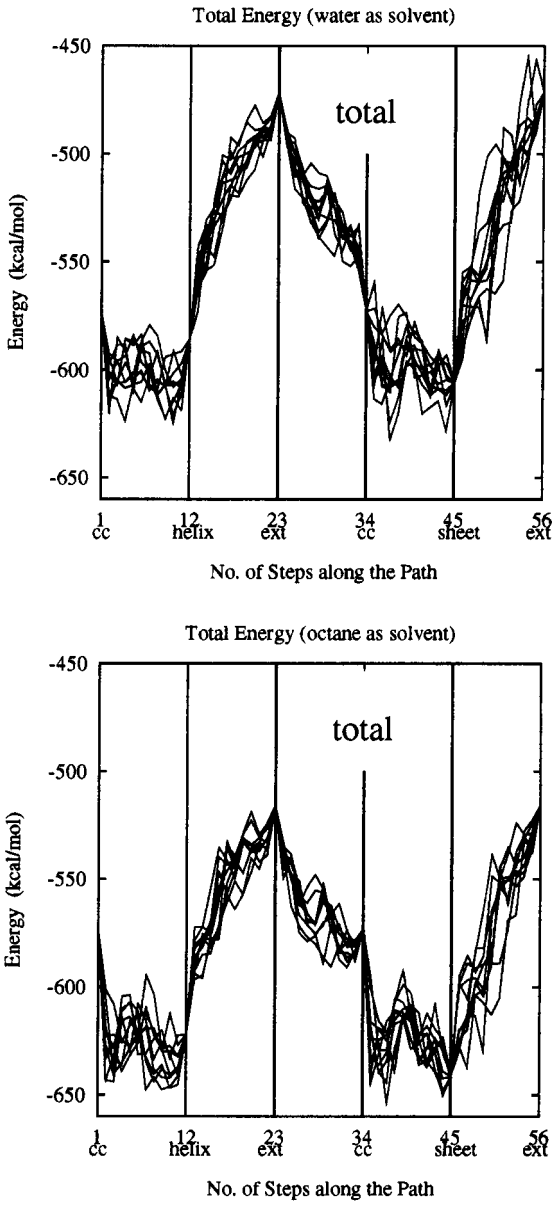

FIGURE 6. Total energy of the peptide along the optimized transition pathways for a bundle of 20 trajectories in both aqueous (upper) and nonaqueous octane (lower) solvent.

5. Energetics of Computed Trajectory "Bundles"

The total effective energy (W), composed of the CHARMM potential energy of the peptide and the solvation energy, is shown for the computed pathways between collapsed coil, helical, sheet, and extended conformations of the peptide. The energetics of the computed pathways is shown for sets of solvation parameters consistent with aqueous solvation or solvation in a nonpolar membrane environment.

5.1 Double Well Energetics of Transition between Stable Compact States. The most important general features of the variation in the total energy over the reaction cycle, shown in Figure 6, are that along any given computed pathway (1) the extended state is highest in energy, (2) the collapsed coil, helical, and folded β-sheet

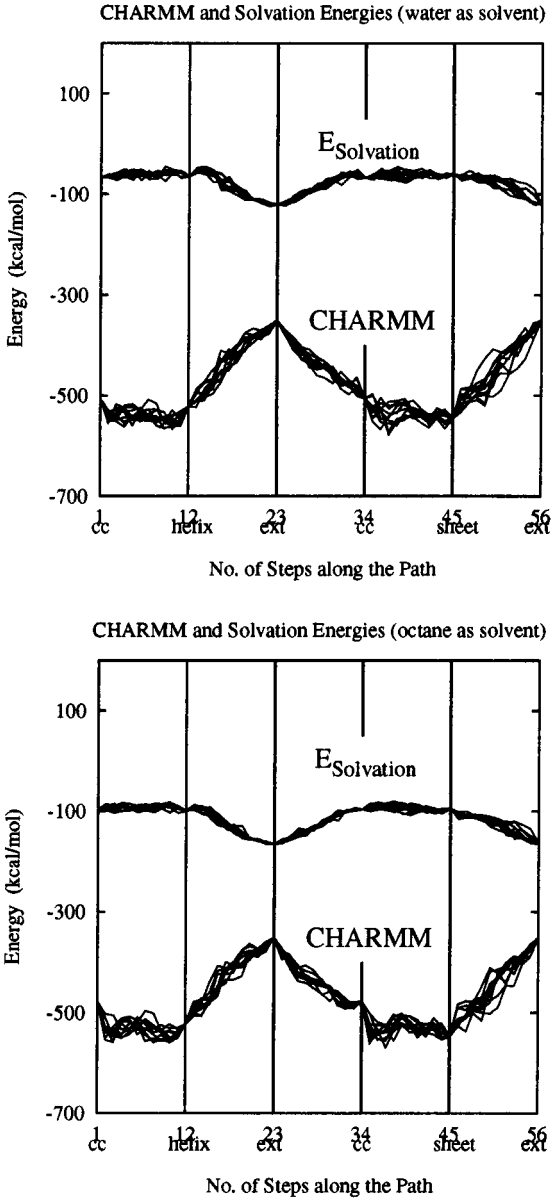

FIGURE 7. Total intrapeptide (CHARMM) energy and separate solvation energy of the peptide along the optimized transition pathways for a bundle of 20 trajectories in both aqueous (upper) and nonaqueous octane (lower) solvent.

conformations are associated with distinct minima in the total energy, and (3) the distinct energy minima associated with the collapsed coil, helical, and folded β-sheet structures are comparable in energy. Note that the initially chosen end point conformations, representing the collapsed coil, helical, and folded β-sheet conformations, taken from the experimentally derived and modeled structures, do not represent energy minima along the transition pathway. Rather, slightly refined structures adjacent to the fixed path end points mark the locations of the minimum energy structures. Rearrangements in the collapsed coil geometry lower the nonbonded peptide energy, shown in Figure 7, while raising slightly the solvation energy by exposing hydrophobic residues and burying the surface area of polar residues. The helical conformation undergoes similar rearrangements to lower the peptide nonbonded interaction energy by burying the hydrophobic surface area, resulting in no significant cost in solvation energy.

5.2 Energetics of the Transition States. On average, we find that the structures in the barrier or transition state regions of the pathways are minima in the solvation energy (see Figure 7). The more open transition state structure exposes polar residues to the solvent, and the favorable associated solvation energy stabilizes the transition state structure. Similarly, the compact collapsed coil and helical (although not the folded β-sheet) structures are local maxima in the solvation energy. This general picture of less compact, solvent-accessible transition states fits the current picture of a "molten globule" conformation. To access the transition state, favorable nonbonded contacts are lost and only slightly compensated for by a more favorable solvation energy.

5.3 Aqueous Solvation Energetics. The collapsed coil is found to have the smallest nonpolar solvent-accessible surface area (see Figure 8). The smaller exposed polar surface area in the collapsed coil geometry explains the higher (less favorable) solvation energy for the collapsed coil relative to the helical conformation. The effect is small in absolute magnitude but large enough to tip the balance in energy slightly in favor of the helical conformation. The energetic barrier separating the collapsed coil and helical minima is on the order of 10−20 kcal/mol.

From the NMR structure analysis, we know that the Aβ(10−35) peptide in water is much more flexible than a typical globular protein. There can be no doubt that the configurational entropy associated with these fluctuations makes a large contribution to the overall free energy. This effect is missing from the effective energy shown in Figure 6. This effect may lead to a stabilization of the collapsed coil conformations relative to the helical conformations. Of course, the greatest entropic stabilization will be in favor of the ensemble of extended coil states.

5.4 Nonpolar (Octane) Solvation Energetics. In our computations, the quasiannealing of the reaction pathways was carried out for the aqueous solvation model. Those optimized pathways were then refined using local energy minimization and the parameters of the nonpolar solvation energetics suitable for solvation in liquid octane (see Section 3). The following general features characterize the differences and similarities between solvation in the aqueous and nonpolar environments. (1) The double-well character of the total energy for the transitions between the collapsed coil and helical or folded β-sheet structures is preserved in the nonpolar environment (see Figure 6). (2) The energy minima associated with the helical conformations in the nonpolar solvation model are deeper relative to the collapsed coil conformations than in the aqueous solvation environment (see Figure 7). The nonpolar solvation environment will better solvate exposed a nonpolar surface of the peptide and stabilize a secondary structure, such as that found in the helical conformations observed for the peptide in nonpolar solvent.[20]

One must be aware that both the peptide model and the solvation model are approximate. The focus of this

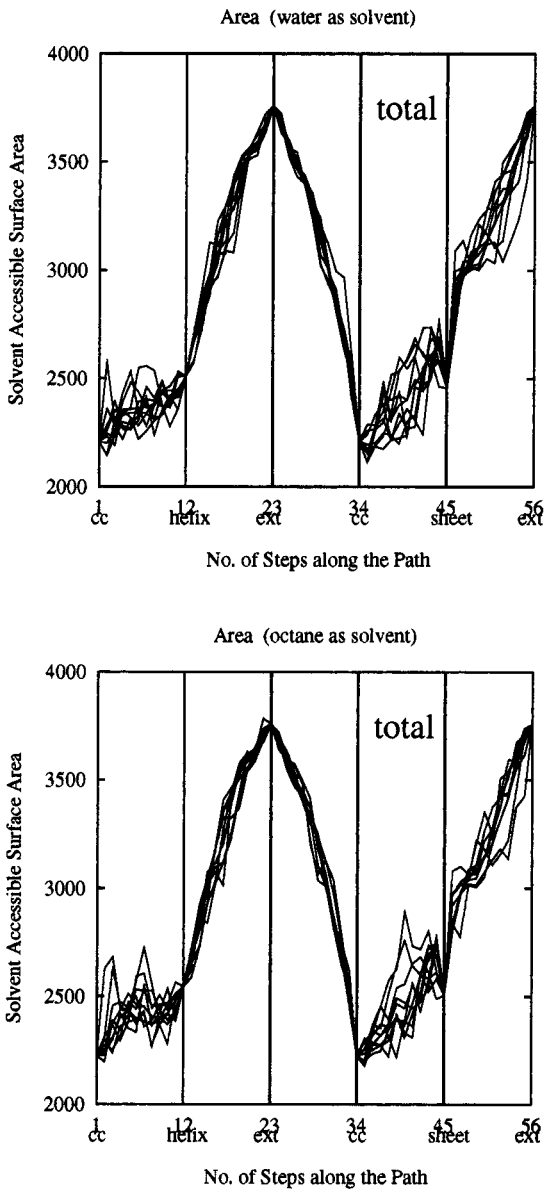

FIGURE 8. Total solvent-accessible surface area of the peptide shown for bundles of 20 trajectories computed for the Aβ-peptide in aqueous (upper) and nonaqueous octane (lower) solvent.

work has been to demonstrate the MaxFlux method by application and to emphasize how aspects of mechanism may be derived from analysis of the resulting trajectory bundles. The general features of the peptide energetics and the similarity in the energies of the collapsed coil and helical structures appear to be consistent with the existing experimental data.

6. Conclusions

In this Account, we have described the MaxFlux algorithm, a general method for the computation of diffusional transition pathways in peptides and proteins, and applied that method to investigate conformational transitions associated with the aggregative activity of the Aβ-peptide. Our results suggest probable transition pathways connecting the collapsed coil, α-helical, folded β-sheet, and extended conformations of the Aβ(10−35)-peptide in aqueous and membrane environments. The principal results for the energetics of the transition pathway are (1) the presence of distinct energy minima, along any given transition pathway, associated with the collapsed coil, α-helical, and folded β-sheet geometries; (2) the stabilization of the minimum energy compact structures by favorable nonbonded interactions; (3) the presence of a significant energy barrier between the sets of compact conformational substates (be it collapsed coil and helical states or collapsed coil and folded β-sheet states); (4) stabilization of the open transition state geometries and by a favorable solvation energy; (5) the prediction that the extended state geometry has a favorable solvation energy relative to the compact coil and helical conformations; and (6) the observation that the collapsed coil conformation has the smallest solvent-accessible surface area of any conformation observed along the computed transition pathways.

Along the transition pathways, we have found a mechanism for formation of the collapsed coil and α-helical geometries from an extended conformation. Each transition pathway includes the early formation of a turn in the region of V24 G25 S26 N27. The same turn region is found to have a relatively well-conserved structure in the collapsed coil and α-helical conformations. These results suggest that the turn may act as a potential nucleus in the formation of collapsed coil and α-helical compact structures in solution. By destabilizing the turn region, the kinetics of the formation of the collapsed coil could be altered. Experimental and theoretical study of the effects of point mutations of residues in this region on the kinetics, structural stability, and plaque competence of the peptide are needed to test this hypothesis.

This work was supported by the National Science Foundation CHE-9975494 (J.E.S.), the National Institutes of Health R01 NS41356-01 (J.E.S.) and R29 AG13735 (J.P.L.), and the Petroleum Research Fund of the American Chemical Society award 34348-AC6 (J.E.S.). J.E.S. is grateful to the Center for Scientific Computing and Visualization at Boston University for computational resources, and to the Institute for Advanced Studies at Hebrew University in Jerusalem for its support and hospitality. We thank Dr. A. E. Roher for providing us with coordinates of the Aβ-peptide model[33] from which we derived the folded β-sheet structure and N. V. Buchete for helpful comments.

References

(1) Mohanty, D.; Elber, R.; Thirumalai, D.; Beglov, D.; Roux, B. Kinetics of peptide folding: computer simulations of SYPFDV and peptide variants in water. *J. Mol. Biol.* **1997**, *272*, 423−442.
(2) Duan, Y.; Kollman, P. A. Pathways to a protein folding intermediate observed in a 1-microsecond simulation in aqueous solution. *Science* **1998**, *95*, 9897−9902.
(3) Duan, Y.; Wang, L.; Kollman, P. A. The early stage of folding of villin headpiece subdomain observed in a 200-nanosecond fully solvated molecular dynamics simulation. *Proc. Natl. Acad. Sci. U.S.A.* **1998**, *282*, 740−744.
(4) Esler, W. P.; Stimson, E. R.; Jennings, J. M.; Vinters, H. V.; Ghilardi, J. R.; Lee, J. P.; Mantyh, P. W.; Maggio, J. E. Alzheimer's disease amyloid propagation by a template-dependent dock-lock mechanism. *Biochemistry* **2000**, *39*, 6288−6295.
(5) Straub, J. E. Reaction rates and transition pathways. In Becker, O., Mackerell, A. D., Roux, B., Watanabe, M., Ed.; *Computational Biochemistry and Biophysics*; Marcel Dekker: New York, 2001.

(6) Huo, S.; Straub, J. E. The MaxFlux algorithm for calculating variationally optimized reaction paths for conformational transitions in many body systems at finite temperature. *J. Chem. Phys.* **1997**, *107*, 5000−5006.
(7) Huo, S.; Straub, J. E. Direct computation of long time processes in proteins: Reaction path study of the coil-to-helix transition in polyalanine. *Proteins* **1999**, *36*, 249−261.
(8) Selkoe, D. J. Alzheimer's disease: a central role for amyloid. *J. Neuropathol. Exp. Neurol.* **1994**, *53*, 438−447.
(9) Selkoe, D. J. Alzheimer's disease: genotypes, phenotypes, and treatments. *Science* **1997**, *275*, 630−631.
(10) Lee, J. P.; Stimson, E. R.; Ghilardi, J. R.; Mantyh, P. W.; Lu, Y.-A.; Felix, A. M.; Llanos, W.; Behbin, A.; Cummings, M.; Criekinge, M. V.; Timms, W.; Maggio, J. E. 1H NMR of Aβ amyloid peptide congeners in water solution. Conformational changes correlate with plaque competence. *Biochemistry* **1995**, *34*, 5191−5200.
(11) Kusumoto, Y.; Lomakin, A.; Teplow, D. B.; Bendek, G. B. Temperature dependence of amyloid beta-protein fibrillization. *Proc. Natl. Acad. Sci. U.S.A.* **1998**, *95*, 12277−12282.
(12) Teplow, D. B. Structural and kinetic features of amyloid beta-protein fibrillogenesis. *Amyloid: Int. J. Exp. Clin. Invest.* **1998**, *5*, 121−142.
(13) Tseng, B. P.; Esler, W. P.; Clish, C. B.; Stimson, E. R.; Ghilardi, J. R.; Vinters, H. V.; Mantyh, P. W.; Lee, J. P.; Maggio, J. E. Deposition of monomeric, not oligomeric, Aβ mediates growth of Alzheimer's disease amyloid plaques in human brain preparations. *Biochemistry* **1999**, *38*, 10424−10431.
(14) Esler, W. P.; Felix, A. M.; Stimson, E. R.; Lachenmann, M. J.; Ghilardi, J. R.; Lu, Y.; Vinters, H. V.; Mantyh, P. W.; Lee, J. P.; Maggio, J. E. Activation barriers to structural transition determine deposition rates of Alzheimer's disease a beta amyloid. *J. Struct. Biol.* **2000**, *130*, 174−183.
(15) Zhang, S.; Iwata, K.; Lachenman, M. J.; Peng, J. W.; Li, S.; Stimson, E. R.; Lu, Y. A.; Felix, A. M.; Maggio, J. E.; Lee, J. P. The Alzheimer's Peptide Aβ Adopts a Collapsed Coil Structure in Water. *J. Struct. Bio.* **2000**, *130*, 130−141.
(16) Massi, F.; Straub, J. E. Energy landscape theory for Alzheimer's amyloid beta-peptide fibril elongation. *Proteins* **2001**, *42*, 217−229.
(17) Massi, F.; Peng, J. W.; Lee, J. P.; Straub, J. E. Simulation study of the structure and dynamics of the Alzheimer's amyloid peptide congener in solution. *Biophys. J.* **2001**, *80*, 31−44.
(18) Barrow, C. J.; Zagorski, M. G. Solution structures of beta peptide and its constituent fragments: relation to amyloid deposition. *Science* **1991**, *253*, 179−182.
(19) Jayawickrama, D.; Zink, S.; Vandervelde, D.; Effiong, R. I.; Larive, C. K. Conformational analysis of the beta-amyloid peptide fragment, beta(12−28). *J. Biomol. Struct. Dyn.* **1995**, *13*, 229−244.
(20) Sticht, H.; Bayer, P.; Willbold, D.; Dames, S.; Hilbich, C.; Beyreuther, K.; Frank, R. W.; Rösch, P. Structure of amyloid A4-(1−40)-peptide of Alzheimer's disease. *Eur. J. Biochem.* **1995**, *233*, 293−298.
(21) Kirschner, D. A.; Abraham, C.; Selkoe, D. J. X-ray diffraction from intraneuronal paired helical filaments and extraneuronal amyloid fibers in Alzheimer disease indicates cross-beta conformation. *Proc. Natl. Acad. Sci. U.S.A.* **1986**, *83*, 503−507.
(22) Inouye, H.; Fraser, P. E.; Kirschner, D. A. Structure of beta-crystallite assemblies formed by Alzheimer beta-amyloid protein analogues: analysis by X-ray diffraction. *Biophys. J.* **1993**, *64*, 502−519.
(23) Barrow, C. J.; Yasuda, A.; Kenny, P. T.; Zagorksi, M. G. Solution conformations and aggregational properties of synthetic amyloid beta-peptides of Alzheimer's disease. Analysis of circular dichroism spectra. *J. Mol. Biol.* **1992**, *225*, 1075−1093.
(24) Fraser, P. E.; Nguyen, J. T.; Surewicz, W. K.; Kirschner, D. A. pH-dependent structural transitions of Alzheimer amyloid peptides. *Biophys. J.* **1991**, *60*, 1190−1201.
(25) Sorimachi, K.; Craik, D. J.; Lloyd, E. J.; Beyreuther, K.; Master, C. L. Identification of a beta-turn in the tertiary structure of a peptide fragment of the Alzheimer amyloid protein. *Biochem. Int.* **1990**, *22*, 447−454.
(26) Coles, M.; Bicknell, W.; Watson, A. A.; Fairlie, D. P.; Craik, D. J. Solution structure of amyloid beta-peptide(1−40) in a water-micelle environment. Is the membrane-spanning domain where we think it is?. *Biochemistry* **1998**, *37*, 11064−11077.
(27) Brooks, B.; Bruccoleri, R.; Olafson, B.; States, D.; Swaninathan, S.; Karplus, M. A program for macromolecular energy, minimization and dynamics calculations. *J. Comput. Chem.* **1983**, *4*, 187−217.
(28) Wesson, L.; Eisenberg, D. Atomic solvation parameters applied to molecular dynamics of proteins in solution. *Protein Sci.* **1992**, *1*, 227−235.
(29) Elber, R. Reaction path studies of biological molecules. In Elber, R., Eds.; *Recent developments in theoretical studies of proteins*; World Scientific: Singapore, 1997.
(30) Elber, R.; Meller, J.; Olender, R. Stochastic path approach to compute atomically detailed trajectories: Application to the folding of C peptide. *J. Phys. Chem. B* **1999**, *103*, 899−911.
(31) Berkowitz, M.; Morgan, J. D.; McCammon, J. A.; Northrup, S. H. Diffusion-controlled reactions: a variational formula for the optimum reaction coordinate. *J. Chem. Phys.* **1983**, *79*, 5563−5565.
(32) Czerminski, R.; Elber, R. Self-avoiding walk between two fixed points as a tool to calculate reaction paths in large molecular systems. *Int. J. Quantum Chem.* **1990**, *24*, 167−186.
(33) Chaney, M. O.; Webster, S. D.; Kuo, Y.-M.; Roher, A. E. Molecular modeling of the Abeta1−42 peptide from Alzheimer's disease. *Prot. Eng.* **1998**, *11*, 761−767.
(34) Molecular Simulations, Inc., 1997.
(35) Nolde, D. E.; Arseniev, A. S.; Vergoten, G.; Efremov, R. G. Atomic solvation parameters for proteins in a membrane environment. Application to transmembrane α-helices. *J. Biomol. Struct. Dyn.* **1997**, *15*, 1−18.
(36) Eisenberg, D.; McLachlan, A. D. Solvation energy in protein folding and binding. *Nature* **1986**, *319*, 199−203.
(37) Wesson, L.; Eisenberg, D. Atomic solvation parameters applied to molecular dynamics of proteins in solution. *Protein Sci.* **1992**, *1*, 227−235.
(38) Efremov, R. G.; Nolde, D. E.; Vergoten, G.; Arseniev, A. S. A solvent model for simulations of peptides in bilayers. I. Membrane-promoting α-helix formation. *Biophys. J.* **1999**, *76*, 2448−2459.
(39) Sorimachi, K.; Craik, D. J. Structure determination of extracellular fragments of amyloid proteins involved in Alzheimer's disease and Dutch-type hereditary cerebral haemorrhage with amyloidosis. *Eur. J. Biochem.* **1994**, *219*, 237−251.
(40) Zhang, S. 1999. Studies of beta-amyloid congeners directed toward understanding the mechanism underlying the formation of amyloid deposits in Alzheimer's disease. Ph.D. Thesis, Boston Univeristy.

AR010031E